

ADIABATIC THERMAL BEAM EQUILIBRIUM IN PERIODIC FOCUSING FIELDS*

C. Chen, MIT, Cambridge, MA 02139, U.S.A.

Abstract

Adiabatic thermal equilibrium is an important state of a charged-particle beam. The rigid-rotor thermal beam equilibrium in a uniform magnetic focusing field is reviewed. The equivalent kinetic and warm-fluid theories of adiabatic thermal beam equilibrium in a periodic solenoidal magnetic focusing field are discussed. Good agreement between theories and experiment is found. Numerical evidence is presented, indicating almost complete elimination of chaotic particle motion in the adiabatic thermal beam equilibrium. The warm-fluid theory of adiabatic thermal beam equilibrium in an alternating-gradient quadrupole magnetic focusing field is discussed.

INTRODUCTION

Exploration of equilibrium states of charged-particle beams and their stability properties is critical to the advancement of basic particle accelerator physics [1-5]. Of particular concern are emittance growth and beam losses which are related to the evolution of charged-particle beams in their non-equilibrium states.

In this paper, we review the rigid-rotor thermal beam equilibrium in a uniform magnetic focusing field [5]. We discuss adiabatic thermal beam equilibrium in a periodic solenoidal magnetic focusing field [1-3]. We show good agreement [2] between the equivalent kinetic and warm-fluid theories and the measurements at the University of Maryland Electron Ring (UMER) [6]. We present the numerical evidence for almost complete elimination of chaotic particle motion in the adiabatic thermal beam equilibrium [7]. We discuss the predictions of the warm-fluid theory of adiabatic thermal beam equilibrium in an alternating-gradient quadrupole magnetic focusing field [3,4].

UNIFORM MAGNETIC FIELD

The thermal equilibrium of a beam of charged particles with charge q and rest mass m propagating at average axial velocity $\beta_b c \hat{e}_z$ in applied uniform magnetic focusing field $\mathbf{B}_0 = B_0 \hat{e}_z$ is a rigid rotor with the equilibrium distribution function [5]

$$f(H, P_\theta, P_z) = C_u \exp\{-(H - \Omega_b P_\theta - c\beta_b P_z)/k_B T\}, \quad (1)$$

where the Hamiltonian H , the canonical angular momentum P_θ and the canonical axial momentum P_z are constants of motion, C and Ω_b are constants, c is the speed of light in vacuum, k_B is the Boltzmann constant,

*Supported by US Department of Energy, Grant No. DE-FG02-95ER40919 and Grant No. DE-FG02-05ER54835.

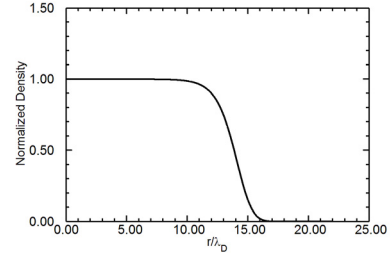


Figure 1: Plot of the normalized density $n_b(r)/n_b(0)$ versus the normalized radius for r/λ_D of a space-charge-dominated beam.

and T is the Kelvin temperature. In the paraxial approximation, we make the following expansion [5]

$$H - \Omega_b P_\theta - c\beta_b P_z - mc^2/\gamma_b \cong \frac{1}{2\gamma_b m} \left[p_r^2 + (p_\theta - \gamma_b m \Omega_b r)^2 + (p_z - \gamma_b m \beta_b c)^2 \right] + \psi(r) \quad (2)$$

where $\gamma_b = (1 - \beta_b^2)^{-1/2}$, \mathbf{p} is the mechanical momentum,

$$\psi(r) = -\frac{1}{2} \gamma_b m \Omega_b \left(\frac{\Omega_c}{\gamma_b} + \Omega_b \right) r^2 + \frac{q}{\gamma_b^2} \phi(r) \quad (3)$$

is an effective potential, the scalar potential ϕ satisfies the Poisson equation

$$\frac{1}{r} \frac{\partial}{\partial r} r \frac{\partial}{\partial r} \phi(r) = -4\pi q n_b(0) e^{-\psi(r)/k_B T}, \quad (4)$$

with the boundary conditions $\phi(0) = 0$ and $\phi'(0) = 0$, $n_b(r) = n_b(0) e^{-\psi(r)/k_B T}$ being the charged-particle density, and $\Omega_c = qB_0/mc$, the cyclotron frequency. It is readily shown that the equilibrium velocity profile of the beam is

$$\mathbf{V}(r) = \Omega_b r \hat{e}_\theta + \beta_b c \hat{e}_z, \quad (5)$$

that is, the beam undergoes rigid rotation as it propagates.

In the *emittance-dominated* regime, we may ignore space-charge effects, and the charged-particle density distribution is a Gaussian distribution, i.e.,

$$n_b(r) = n_b(0) \exp\left[\frac{\gamma_b m \Omega_b}{2k_B T} \left(\frac{\Omega_c}{\gamma_b} + \Omega_b \right) r^2 \right]. \quad (6)$$

In the *space-charge-dominated* regime, the charged-particle density is flat near the beam axis and drops off rapidly within a few Debye lengths at the beam edge, as illustrated in Fig. 1, where $\lambda_D \equiv \sqrt{\gamma_b^2 k_B T / 4\pi q^2 n_b(0)}$ is the Debye length.

PERIODIC SOLENOIDAL FIELD

We consider a thin, continuous, axisymmetric ($\partial/\partial\theta = 0$), charged-particle beam, propagating with axial velocity $\beta_b c \hat{e}_z$ through the magnetic focusing field

$$\mathbf{B}_0(r, s) = -\frac{1}{2}B'_z(s)r\hat{\mathbf{e}}_r + B_z(s)\hat{\mathbf{e}}_z, \quad (7)$$

where $s = z$ is the axial coordinate, the prime denotes the derivative with respect to s , and $B_z(s)$ is the axial magnetic field which can be either periodic along the z -axis with periodicity S or an arbitrary function of s .

Because the beam is axisymmetric, the canonical angular momentum P_θ is a constant of motion, i.e.,

$$dP_\theta / ds = 0. \quad (8)$$

After performing a two-step canonical transformation [2,3], we have also found that the scaled transverse Hamiltonian for the single-particle motion [2,3]

$$\bar{E} \equiv w^2(s)\bar{H}_\perp(\bar{x}, \bar{y}, \bar{P}_x, \bar{P}_y, s) \quad (9)$$

is an approximate invariant (see [2,3] for detailed analyses and definitions of $w(s)$, \bar{H}_\perp , \bar{x} , \bar{P}_x , \bar{P}_y , etc.). We have chosen the beam equilibrium distribution in the form similar to the Maxwell-Boltzmann distribution

$$f_b = C \exp[-\beta(\bar{E} - \omega_b \bar{P}_\theta)], \quad (10)$$

where C , β and ω_b are constants. C is an integration constant, β is related to the beam emittance, and ω_b is a measure of the beam rotation frequency relative to the Larmor frame. The distribution function f_b defined in Eq. (10) is also a Vlasov equilibrium, i.e., $\partial f_b / \partial s = 0$. An equivalent warm-fluid beam equilibrium theory [1,3] has also been developed. Both theories make the following two important predictions [1-3]:

1. The thermal beam emittance is a constant, i.e.,

$$\varepsilon_{th}^2 \equiv \frac{\langle x^2 \rangle}{\beta_b^2 c^2} \langle (v_x - V_x)^2 \rangle = \frac{k_B T_\perp(s) r_{brms}^2(s)}{2\gamma_b m \beta_b^2 c^2} = const. \quad (11)$$

2. The equation of state is adiabatic, i.e.,

$$T_\perp(s) r_{brms}^2(s) = const. \quad (12)$$

The rms envelope equation is

$$\frac{d^2 r_{brms}}{ds^2} - \frac{\Omega_b(s)}{\beta_b^2 c^2} \left[\Omega_b(s) + \frac{\Omega_c(s)}{\gamma_b} \right] r_{brms} - \frac{K}{2r_{brms}} = \frac{4\varepsilon_{th}^2}{r_{brms}^3}, \quad (13)$$

where $\Omega_b(s) = 2\omega_b \varepsilon_{th} \beta_b c / r_{brms}^2(s) \sqrt{1 - \omega_b^2} - \Omega_c(s) / 2\gamma_b$, ω_b is a constant, $\Omega_c(s) = qB_z(s) / mc$ is the local cyclotron frequency, and $K = 2q^2 N_b / \gamma_b^3 \beta_b^2 mc^2$ is the normalized beam perveance. The beam density profile is

$$n_b(r, s) = \frac{4\pi C \varepsilon_{th}^2}{r_{brms}^2(s)} \exp \left\{ -\frac{Kr^2}{8\varepsilon_{th}^2} - \frac{r^2}{r_{brms}^2(s)} - \frac{q\phi(r, s)}{\gamma_b^2 k_B T_\perp(s)} \right\}, \quad (14)$$

where the scalar potential for the self-electric field is determined by the Poisson equation

$$\frac{1}{r} \frac{\partial}{\partial r} \left(r \frac{\partial \phi}{\partial r} \right) = -4\pi q n_b(r, s). \quad (15)$$

By solving Eqs. (13)-(15), we have calculated the beam transverse density profile of the UMER 5 keV, 6.5 mA electron beam at $s = 17.2$ cm, as shown in solid curve in Fig. 2. The dashed curve is the equivalent KV-type beam density profile. Compared with the experimental

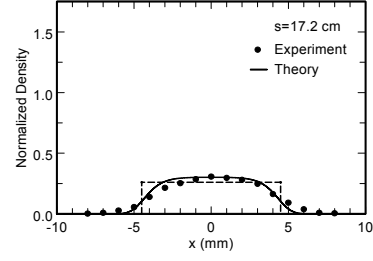


Figure 2: Normalized beam transverse density profiles of a 5 keV, 6.5 mA ($4\varepsilon_{rms} = 30$ mm-mrad) electron beam at $s = 17.2$ cm. The solid curve is from theory, the dotted curve is the experimental measurements, and the dashed line is the equivalent KV beam density distribution.

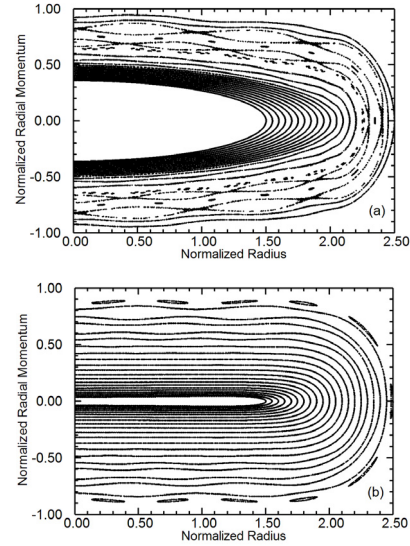


Figure 3: Poincare surface-of-section maps of charged-particle trajectories in a) KV-type beam equilibrium and b) adiabatic thermal beam equilibrium for $P_\theta = 0$. Here, the choice of system parameters corresponding to $P_\theta = 0$, $S\sqrt{\kappa_z(s)} = (2/3)^{1/2} \sigma_0 [1 + \cos(2\pi s/S)]$, vacuum phase advance $\sigma_0 = 80^\circ$, $\omega_b = 0$ [or $\Omega_b(s) = -\Omega_c(s) / 2\gamma_b$], and $SK / 4\varepsilon_{th} = 7.0$. The normalized radial momentum is $(S / 4\varepsilon_{th})^{1/2} dr / ds$ and the normalized radius is $r / \sqrt{4\varepsilon_{th} S}$.

measurements (dotted curve) [6], the calculated beam density profile [2] is in good agreement.

Figure 3 shows a comparison between the Poincare surface-of-section maps of charged-particle trajectories in a) KV-type beam equilibrium and b) adiabatic thermal beam equilibrium [7]. They are generated by plotting (r, P_r) as a trajectory arrives at the lattice points $s/S = 0, 1, 2, \dots, 2000$. Comparing Fig. 3(a) with Fig. 3(b), there are three important differences to note [7]. First, the action of a charged particle in the KV-type beam is larger than that in the adiabatic thermal beam. Second, there are chaotic seas in the phase space of the KV-type beam

equilibrium, whereas chaotic motion is almost completely eliminated in the phase space of the adiabatic thermal beam equilibrium. Third, the widths of the nonlinear resonances in the adiabatic thermal beam equilibrium are narrower than those in the KV-type beam equilibrium.

QUADRUPOLE FIELD

The applied alternating-gradient quadrupole magnetic focusing field inside the beam can be approximated by

$$\mathbf{B}_0(x, y, s) = B'_q(s)(y\hat{\mathbf{e}}_x + x\hat{\mathbf{e}}_y), \quad (16)$$

where $s = z$ is the axial coordinate, prime denotes the derivative with respect to z , $B'_q(s) \equiv \partial B_x / \partial y|_{(0,0,s)} = \partial B_y / \partial x|_{(0,0,s)}$ is the field gradient coefficient which is periodic along the z -axis with periodicity S , i.e., $B'_q(s) = B'_q(s + S)$. The main predictions of the warm-fluid equilibrium theory are:

First, the equilibrium density and the potential for the equilibrium self-electric field are determined self-consistently from the Poisson equation

$$\begin{aligned} \frac{\partial^2 \phi(x, y, s)}{\partial x^2} + \frac{\partial^2 \phi(x, y, s)}{\partial y^2} = & -\frac{4\pi q C_q}{x_{brms}(s)y_{brms}(s)} \\ & \times \exp\left(-\frac{K[y_{brms}(s)x^2 + x_{brms}(s)y^2]}{4\epsilon_{4Dth}^2[x_{brms}(s) + y_{brms}(s)]}\right) \\ & \times \exp\left(-\frac{x^2}{2x_{brms}^2(s)} - \frac{y^2}{2y_{brms}^2(s)} - \frac{q\phi(x, y, s)}{\gamma_b^2 k_B T_\perp(s)}\right) \end{aligned} \quad (17)$$

where the 4D rms thermal emittance ϵ_{4Dth} defined by

$$\epsilon_{4Dth}^4(s) \equiv (\beta_b c)^{-4} \langle x^2 \rangle_\Gamma \langle y^2 \rangle_\Gamma \langle (v_x - V_x)^2 \rangle_\Gamma \langle (v_y - V_y)^2 \rangle_\Gamma \quad (18)$$

is shown to be a constant, i.e.,

$$\epsilon_{4Dth} = \left[\frac{k_B T_\perp(s) x_{brms}(s) y_{brms}(s)}{m \gamma_b \beta_b^2 c^2} \right]^{1/2} = const., \quad (19)$$

the rms beam envelopes $x_{brms}(s)$ and $y_{brms}(s)$ correspond to matched solutions to the self-consistent rms envelope equations

$$x_{brms}'' + \kappa_q(s)x_{brms} - \frac{K}{2(x_{brms} + y_{brms})} = \frac{\epsilon_{4Dth}^2}{x_{brms}^2 y_{brms}} \quad (20)$$

and

$$y_{brms}'' - \kappa_q(s)y_{brms} - \frac{K}{2(x_{brms} + y_{brms})} = \frac{\epsilon_{4Dth}^2}{y_{brms}^2 x_{brms}}, \quad (21)$$

and the constant C_q is determined by a procedure described in [3,4].

Second, the constant-density contours and equipotential contours are ellipses [3,4]. However, the density profile does not satisfy the simplest elliptical symmetry condition which was a key assumption in the derivation of the well-known rms envelope equations [8]. This is illustrated in Fig. 4 for an adiabatic thermal beam with $\hat{K} = SK / 4\epsilon_{4Dth} = 4$ at $s = 0$ in a step-function lattice $\kappa_q(s) = \kappa_q(s + S)$ with a filling factor of $\eta = 0.3$ and a

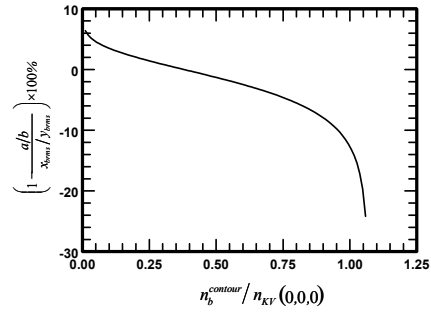


Figure 4: Plot of the difference between the ratio of the semi-axis of the contours of constant density and the ratio of the rms envelopes sizes in percent. Here, the parameters are $\hat{K} = SK / 4\epsilon_{4Dth} = 4$ at $s = 0$ in a step-function lattice $\kappa_q(s) = \kappa_q(s + S)$ with a filling factor of $\eta = 0.3$ and a strength of $S^2 \kappa_q(0) = 15$.

strength of $S^2 \kappa_q(0) = 15$, where the percentage difference between the ratio of the semi-axes of constant-density contour, a/b , and the ratio of the rms envelopes, x_{brms} / y_{brms} , is plotted as a function of the density.

CONCLUSION

Adiabatic thermal equilibrium of a charged-particle beam was discussed. The rigid-rotor thermal beam equilibrium in a uniform magnetic focusing field was reviewed. The kinetic and warm-fluid theories of adiabatic thermal beam equilibrium in a periodic solenoidal magnetic focusing field were discussed. Agreement between theory and experiment was found. Numerical evidence was presented, indicating almost complete elimination of chaotic particle motion in the adiabatic thermal beam equilibrium. The key predictions of the warm-fluid theory of adiabatic thermal beam equilibrium in an alternating-gradient quadrupole magnetic focusing field were discussed.

REFERENCES

- [1] K. R. Samokhvalova, J. Zhou, and C. Chen, Phys. Plasmas **14**, 103102 (2007).
- [2] J. Zhou, K. R. Samokhvalova, and C. Chen, Phys. Plasmas **15**, 023102 (2008).
- [3] K. R. Samokhvalova, *Thermal Equilibrium Theory of Periodically Focused Charged-Particle Beams*, Ph.D Thesis, Massachusetts Institute of Technology, 2008.
- [4] K. R. Samokhvalova, J. Zhou, and C. Chen, Phys. Plasmas **16**, 043115 (2009).
- [5] R. C. Davidson and H.S. Uhm, Phys. Fluids **22**, 1375 (1979).
- [6] S. Bernal, B. Quinn, M. Reiser, and P.G. O'Shea, Phys. Rev. ST Accel. Beams **5**, 064202 (2002).
- [7] H. Wei and C. Chen, Phys. Rev. ST Accel. Beams **14**, 024201 (2011).
- [8] F.J. Sacherer, IEEE Trans. Nucl. Sci. **18**, 1105 (1971).